


# Mechanical and Durability Characteristics of One-Part Alkali-Activated Mortars Incorporating Volcanic and Industrial Waste Materials

ISSN: 2576-8840



**\*Corresponding author:** KMA Hossain, Professor, Department of Civil Engineering, Toronto Metropolitan University, 350 Victoria Street, Toronto, ON, M5B 2K3, Canada

**Submission:**  September 25, 2023

**Published:**  October 05, 2023

Volume 19 - Issue 4

**How to cite this article:** KMA Hossain\*. Mechanical and Durability Characteristics of One-Part Alkali-Activated Mortars Incorporating Volcanic and Industrial Waste Materials. Res Dev Material Sci. 19(4). RDMS. 000967. 2023. DOI: [10.31031/RDMS.2023.19.000967](https://doi.org/10.31031/RDMS.2023.19.000967)

**Copyright@** KMA Hossain, This article is distributed under the terms of the Creative Commons Attribution 4.0 International License, which permits unrestricted use and redistribution provided that the original author and source are credited.

**KMA Hossain\***

Department of Civil Engineering, Toronto Metropolitan University, Canada

## Abstract

Ambient-cured Alkali-Activated Mortars (AAMs) are developed incorporating Volcanic Ash (VA), powdered pumice (VP), ground granulated blast furnace slag (GGBFS) and their combinations. Powder form alkaline reagent (calcium hydroxide: sodium metasilicate = 1:2.5), silica sand and a one-part dry mixing method were used. The mechanical (dry density, compressive strength, ultrasonic pulse velocity, and fracture energy), durability (shrinkage/expansion and mass change in water curing condition, water absorption/sorptivity and rapid chloride permeability) and microstructural (SEM/EDS analyses) characteristics of six AAMs were investigated. The 28-day compressive strengths of AAMs ranged from 29MPa to 49MPa with 100%GGBFS showing the highest value. Incorporation of VA/VP produced lower compressive strength, UPV, fracture energy and shrinkage characteristics but higher sorptivity and chloride permeability compared to their GGBFS counterparts. This can be attributed to the lower activation potential of VA/VP producing less dense microstructure which is characterized by predominant formation of C-A-S-H and N-C-A-S-H binding phases in all AAMs. This study confirmed the viability of producing cement-free VA and VP based AAMs (ranging from normal weight to lightweight) having satisfactory mechanical and durability characteristics for construction applications.

**Keywords:** Alkali activated mortars; Volcanic materials; Industrial wastes; Powder form reagents; Strength; Fracture; Durability; Microstructure

## Introduction

The alkali-activated materials are developed by activation of aluminosilicate rich industrial wastes or natural pozzolans (known as precursors) through alkaline reagents [1-3]. These cement-free materials are more sustainable and greener (with low embodied energy) than the currently available cement-based concrete composites. Researches have been conducted on the development alkali-activated binders, mortars (with fine aggregates) and concrete (with fine and coarse aggregates) incorporating industrial wastes (such as fly ash, blast furnace slag (GGBFS), metakaolin, glass powder etc.) over the last decade [1-5]. The fresh state, mechanical (strength, fracture) and durability (drying shrinkage, permeability, freeze-thaw etc.) properties of these materials had been extensively investigated by studying the influence of types and combinations of reagents, materials, mixing techniques (one part dry or two-part solution-based) and curing (ambient or heat-cured) conditions. The influence of mix composition (types and proportion of precursors, concentration and silica modulus of alkali solutions, liquid to binder ratio) on strength and fracture energy characteristics of GGBFS/FA/metakaolin-based binders/concrete was investigated [6-9].

The influence of precursors (fly ash, slag, MgO, paper sludge, glass powder) on drying shrinkage of alkali-activated concrete was investigated under varying curing conditions [10-14]. The effect of heat curing and ambient curing of alkali-activated slag and fly ash concretes

(on drying shrinkage at early and later ages was investigated. The shrinkage strains of Fly Ash (FA) incorporated alkali-activated concretes were observed to be lower than their slag counterparts [15]. The water permeability and Ultrasonic Pulse Velocity (UPV) of low calcium fly ash and slag incorporated alkali-activated concretes were also investigated [16]. The water absorption rate was found to be higher in mixes incorporating FA and GGBFS than the GGBFS alone mixes with the highest sorptivity indices were observed for the mixtures using FA. Also, lower UPV values were observed for mixes with increased FA content due to lower activation potential of FA [17].

The literature review suggests that there has been limited research on the development and performance evaluation (based on mechanical, durability and microstructural characteristics) of Alkali-Activated Mortars (AAMs) incorporating volcanic materials [2,18-20]. Volcanic materials with large amount of silica and alumina, may be considered as feedstock for alkali-activated materials and geopolymers. The relatively low reactivity of these materials because of the low amount of amorphous phase can be a limitation [21,22]. However, this can be improved by controlling fineness, amount of highly reactive GGBFS or activation with highly concentrated alkaline reagents.

This paper addresses the above-mentioned research gaps (as new contributions) by presenting the results of a novel study on the development and comprehensive evaluation of volcanic ash (VA) and finely ground pumice (VP) incorporated AAMs made in combination with GGBFS (0%, 50% and 100%), powder form reagents (calcium hydroxide + sodium metasilicate) and ambient curing conditions. The mechanical, durability and microstructural characteristics of AAMs have been investigated. Volcanic activities are common and volcanic debris such as: VA and VP are found abundantly in many parts of the world. This research is put forward in an attempt to explore the possible utilization of volcanic materials for producing zero-cement based green AAMs. This research will also lead to the meaningful utilization of these natural resources and also reduce environmental hazards. The findings of this research will certainly benefit engineers and researchers to understand the properties of developed VA/VP based AAMs and further develop such AAM based concrete and composites for construction applications.

## Experimental Program, Materials and Methods

The experimental program involved the development of AAMs incorporating volcanic materials (VA and VP) with industrial waste (GGBFS) as source materials or precursors and assessment of their mechanical (dry density, compressive strength, ultrasonic pulse velocity and fracture energy), durability (drying shrinkage in water curing regime, sorptivity and rapid chloride permeability) and microstructural properties through Scanning Electron Microscopy (SEM) coupled with energy-dispersive X-ray spectroscopy (EDS).

### Materials

Volcanic Ash (VA), finely ground Volcanic Pumice (VP), Ground Granulated Blast Furnace Slag (GGBFS), silica sand (maximum

particle size 600 $\mu$ , retained 2.2% and 0.4% retained on 2700  $\mu$ ) having 99.88% SiO<sub>2</sub> and a powder-based reagent were used to develop AAM mixes using the dry mixing technique [23]. Reagent or activator was composed of a combination of calcium hydroxide (Ca(OH)<sub>2</sub>) and sodium meta-silicate (Na<sub>2</sub>SiO<sub>3</sub>.5H<sub>2</sub>O), having a modular ratio (SiO<sub>2</sub>/Na<sub>2</sub>O) of 1.0. The specific gravities of Ca(OH)<sub>2</sub> and Na<sub>2</sub>SiO<sub>3</sub>.5H<sub>2</sub>O were 2.24 and 1.81g/cm<sup>3</sup>, respectively. The alkalinity in terms of pH values of Ca(OH)<sub>2</sub> and Na<sub>2</sub>SiO<sub>3</sub>.5H<sub>2</sub>O were 12.4-12.6 and 14, respectively. A polycarboxylate ether-based superplasticizer having a pH of 6, a specific gravity of 1.06 g/cm<sup>3</sup> and an approximate solid content of 40% was used as a high range water reducer admixture (HRWRA) to produce flowable mortar mixes. The chemical and the physical properties of VA, VP and GGBFS are presented in Table 1.

**Table 1:** Chemical composition and physical characteristics source materials or precursors.

Chemical Composition (%)	VA	VP	GGBFS
SiO <sub>2</sub>	59.3	60.82	35.97
Al <sub>2</sub> O <sub>3</sub>	17.5	22.09	9.18
Fe <sub>2</sub> O <sub>3</sub>	7.0	7.04	0.50
CaO	6.1	4.44	38.61
MgO	2.6	1.94	10.99
K <sub>2</sub> O	2.0	2.25	0.36
Na <sub>2</sub> O	3.1	3.42	0.28
MnO	-	-	0.25
TiO <sub>2</sub>	-	-	0.39
P <sub>2</sub> O <sub>5</sub>	-	-	0.01
SO <sub>3</sub>	0.7	0.14	-
LOI	1.0	1.52	0.74
Physical properties	VA	VP	GGBFS
Density (g/cm <sup>3</sup> )	2.45	0.87 (bulk)	2.87
Retained on 45 $\mu$ (%) Blaine fineness (m <sup>2</sup> /kg)	2.7 (on 75 $\mu$ ) 315	2.5 (on 75 $\mu$ ) 285	<5 489.30

### Mix proportions

Six one-part optimized AAM mixtures were developed with a constant amount of silica sand and their mix proportions are presented in Table 2. SM, VAM, VPM mixes were developed by using 100% GGBFS, VA and VP, respectively, 50% VA + 50%VP (by mass of the total binder content) was used for VAVP mix, 50%VA+50%GGBFS for VASM mix and 50%VP+50%GGBFS for VPSM mix as indicated in Table 2. The reagent to binder ratio of powder-based reagent was kept constant at 0.1. A constant amount of silica sand (30% by mass of total binder content) was used with a constant water to binder ratio of 0.35 which provided a minimum slump flow diameter of 150mm. The dosage of HRWRA was kept constant at 0.02. The reagent component and the initial chemical ratios in the mix compositions are presented in Table 3. The reagent has a reagent component ratio (calcium hydroxide to sodium metasilicate) of 1:2.5. These component ratios were superior performing in terms of compressive strength from authors' research [23].

**Table 2:** Mix proportions for one-part alkali activated mortars.

Mix -des.	Total SCMs (Binder*)	Cement	VA	VP	GGBFS (S)	Reagent/Binder	Silica Sand	Water/Binder	HRWRA**
<b>Alkali activated mortars (AAMs)- CS: Binary and CFS: Ternary</b>									
SM	1	0	0	0	1.00	0.1	0.3	0.35	0.02
VAM	1	0	1.00	0	0	0.1	0.3	0.35	0.02
VPM	1	0	0	1.00	0	0.1	0.3	0.35	0.02
VAVPM	1	0	0.50	0.50	0	0.1	0.3	0.35	0.02
VASM	1	0	0.50	0	0.50	0.1	0.3	0.35	0.02
VPSM	1	0	0	0.50	0.50	0.1	0.3	0.35	0.02
All numbers are mass ratios of the binder									
*Binder denotes supplementary cementitious materials (SCMs: VA-volcanic pumice, VP: finely ground volcanic pumice or GGBFS: ground granulated blast furnace slag)									
** HRWRA: Poly-carboxylate ether-based superplasticizer									

**Table 3:** Reagent component and chemical ratios in mix compositions.

Mix Designation	Reagent Component Ratio	Chemical Ratios (SCMs + Reagents)			
		SiO <sub>2</sub> /Al <sub>2</sub> O <sub>3</sub>	Na <sub>2</sub> O/SiO <sub>2</sub>	CaO/SiO <sub>2</sub>	Na <sub>2</sub> O/Al <sub>2</sub> O <sub>3</sub>
SM	1:2.5	2.52	0.10	0.86	0.26
VAM	1:2.5	2.71	0.085	0.67	0.17
VPM	1:2.5	2.68	0.085	0.66	0.17
VAVPM	1:2.5	2.69	0.08	0.67	0.16
VASM	1:2.5	2.58	0.09	0.78	0.21
VPSM	1:2.5	2.56	0.09	0.78	0.21

The fundamental chemical ratios in terms of silicon oxide to aluminum oxide, sodium oxide to silicon oxide, calcium oxide to silicon oxide and sodium oxide to aluminum oxide were evaluated from the XRF results of the precursors/source materials and the chemical composition of the reagents. These chemical ratios are found to fall within the range of AAMs with adequate workability and strength characteristics as per recent studies on fly ash and slag-based mortars [2].

### Mixing, casting, and curing of specimens

The source materials (binder constituents) and the reagent required for each mix composition were weighed per the proportions given in Table 2 and Table 3. The reagent components were first mixed thoroughly to form a multi-component reagent/activator and then added to the rigorously blended binder constituents. The total binder system was then dry mixed for about 3 minutes in a shear mixer and then two-third of the required water was gradually added to the mix. The HRWRA mixed with the remaining amount of water was gradually added to make the paste flowable for the addition of silica sand as per the proportions given in Table 2. The incorporation of sand was followed once the paste became flowable so that the sand did not hinder the initial alkali activation reactions taking place. After sand addition, the remaining HRWRA mixed with water was added gradually to the mortar. The total mixing procedure lasted about 12-15 minutes.

At least 18 cube specimens having dimensions of 50mm × 50mm × 50mm were prepared for each mix composition for compressive strength testing. Three mortar beam specimens having

dimensions of 50.8mm × 76.2mm × 355.6mm per mix composition were prepared for fracture energy characteristics and ultra-sonic pulse velocity (UPV) measurements. A notch of depth equal to half the beam depth was created to make sure the crack occurs and propagates from the center of the beam specimens. Prisms with dimensions (25mm × 25mm × 285mm) were prepared for shrinkage/expansion and mass change investigations. The cylinders (100mm × 200mm) were cast for conducting the sorptivity measurements on the disc specimens (100mm × 50mm) cut out of cylinders at the testing days. The beam specimens (50.8mm × 76.2mm × 355.6mm) were prepared for testing resistance to freeze-thaw cycles. All the specimens were kept in the curing room/chamber maintained at a temperature of 23±3 °C and 95±5% Relative Humidity (RH) unless other conditions were required as per the test methods. The molds were de-molded 24 hours after casting and were kept in the curing chamber until the testing days.

### Test methods

The compressive strength test at 28/56 days was conducted on cube specimens according to ASTM C109/C109M-2016 [24]. A three-point loading fracture test (as shown in Figure 1) was conducted on notched beam specimens (50.8mm × 76.2mm × 355.6mm) to evaluate the fracture energy ( $G_f$ ) as per RILEM TC50-FMC [8]. A constant span to beam depth ratio ( $l/d$ ) of 4 and an initial notch depth to beam depth ratio ( $a/d$ ) of 0.5 was implemented for all the specimens. The displacement control rate of 0.18mm/min was used to ensure that the maximum load for any specimen occurs within the initial 30-60 seconds.

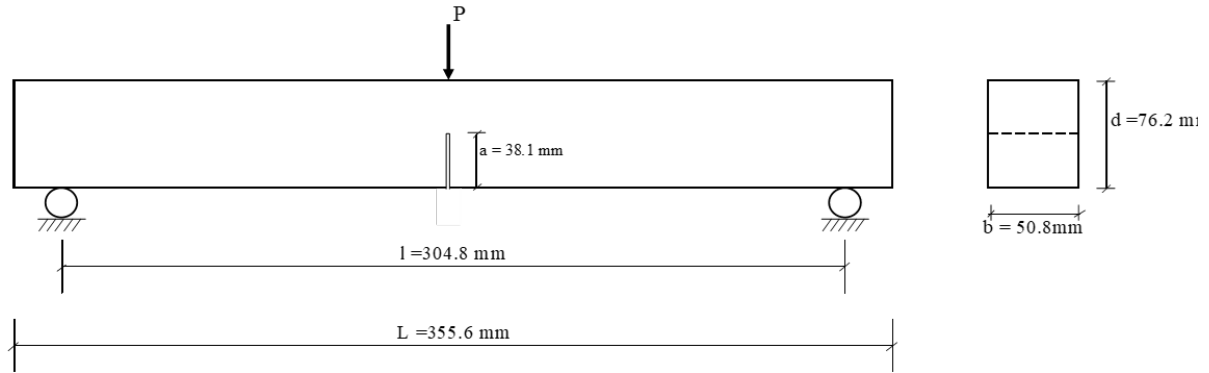


**Figure 1:** Schematic sketch of fracture energy test set-up.

Fracture energy ( $G_f$ ) defined as the energy consumed during the creation of one unit area of the crack can be determined as per RILEM TC50-FMC [8] by Eq. 1:

$$(1) \quad G_f = \frac{(W_0 + mg\delta_0)}{A_{lig}}$$

where  $W_0$  is the area under the load-displacement curve of the three-point bending test;  $m$  is the mass of the beam specimen between the supports as illustrated in Figures 2(a-b);  $g$  is the acceleration due to gravity ( $9.8\text{m/s}^2$ );  $\delta_0$  is the final displacement at failure and  $A_{lig}$  is the area of the ligament ( $\text{m}^2$ ).

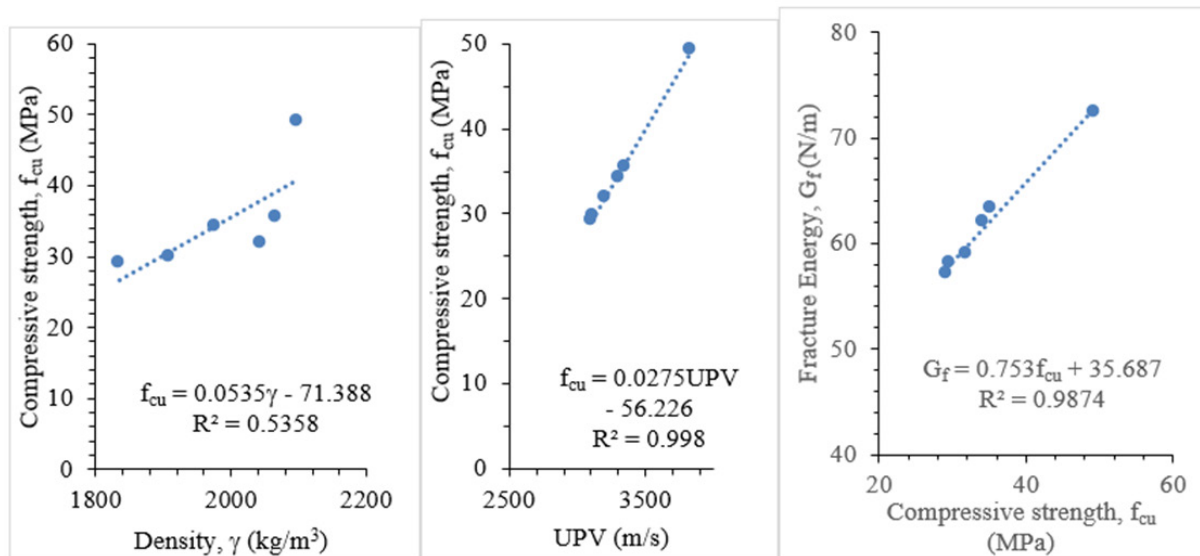


**Figure 2:** Relationships between UPV, compressive strength and dry density at 28 days.

The drying shrinkage test was conducted in compliance with ASTM C157/157M -2017 [25]. Eight prismatic specimens with dimensions 25mm x 25mm x 285mm were prepared for each mix composition and de-moulded after 24 hours. The specimens were stored in air-tight plastic bags until being de-moulded. After demolding, initial mass and length readings were taken with a digital comparator having an accuracy of up to 0.001mm and considered a reference. The length and mass change readings were taken at 1/7/28/56/90 days for the specimens subjected to water curing regime in compliance with ASTM C157/157M-2017 [25]. In the water curing regime, specimens were kept immersed in water through the days of testing.

The water absorption rate (sorptivity index) was determined in compliance with ASTM C1585-13 (2013) [26]. For each mix,

six specimens were prepared by cutting  $\text{Ø}100\text{mm} \times 50\text{mm}$  discs from the exterior parts of  $\text{Ø}100\text{mm} \times 200\text{mm}$  cylinders. The specimens were cured for 21 days in air-tight plastic bags at an ambient temperature of  $23\pm 2^\circ\text{C}$  and  $95\pm 5\%$  Relative Humidity (RH). After the curing period, the specimens were placed inside an oven maintained at a temperature of  $50\pm 2^\circ\text{C}$  for 3 days and later transferred to a sealable air-tight container for the next 15 days before initiating the water absorption process. Following the ASTM guidelines, specimens were kept submerged in water to a depth of  $2\pm 1\text{mm}$  from their bottom surface. An aluminum tape sealed the sides of the specimens, and the top surface of specimens was covered with plastic wrap to prevent the evaporation of water. The sorptivity test was performed at the age of 39 days, consisting of 21 days of curing period and 18 days of specimens' preparation. The



sorptivity index is based on the rate of water penetration through unsaturated concrete by capillary suction. Thus, the specimens' mass was recorded at standard time intervals during testing, and mass change was evaluated to determine the initial and secondary sorptivity indices.

Rapid Chloride Permeability (RCP) tests were conducted in accordance with ASTM standard ASTM C1202-22E01 (2022) [27] on cylindrical specimens with a diameter of 100mm and 50mm height at 28 days. The current passing through the setup was recorded using a data acquisition system, and the total charge was obtained from the average of three specimens evaluated for each AAM mixture. The mixes were classified based on ASTM C1202-22E01 (2022) [27].

**Table 4:** Mechanical characteristics of AAMs.

Mix Designation	Density (kg/m <sup>3</sup> )	Compressive strength, $f_{cu}$ (MPa)		UPV (m/s)	Fracture Energy
	28d	28d	56d	28d	N/m
SM	2098 ± 20	49.2 ± 1.82	54.2 ± 1.48	3832 ± 43	72.4 ± 2.1
VAM	2045 ± 22	32.0 ± 1.33	36.5 ± 1.32	3202 ± 36	59.1 ± 1.5
VPM	1825 ± 10	29.2 ± 1.51	32.5 ± 1.28	3111 ± 42	57.2 ± 1.2
VAVPM	1910 ± 19	29.8 ± 1.32	33.1 ± 1.21	3121 ± 32	58.1 ± 1.3
VASM	2065 ± 21	35.4 ± 1.19	38.2 ± 1.23	3345 ± 39	63.2 ± 1.2
VPSM	1975 ± 22	34.2 ± 1.23	36.1 ± 1.35	3312 ± 43	62.1 ± 1.3

**Dry density, compressive strength and UPV:** Dry density, compressive strength, UPV and fracture energy of AAM mixes are presented in Table 4. All the mixes satisfied the criteria for structural concrete as per ACI 318 [28,29], exhibiting 28-day compressive strengths ranging from 29MPa to 49MPa. The SM mix with 100%GGBFS obtained the highest 28-day compressive strength of 49MPa amongst all AAMs, as noted in Table 4. Incorporation of VA and VP as replacement of GGBFS decreased the compressive strength. Generally, compressive strength of AAMs decreased with the increase of VA or VP. VA and VP incorporated mixes exhibited comparable compressive strength (Table 2) with VP mixes showing lower density as expected. From 28 days to 56 days, 6% to 14% increase in compressive strength was observed in AAMs due to the ongoing formation of CSH binding phases/gels with maximum increase observed in 100%GGBFS mix. The fracture energy and UPV of AAMs varied from 57N/m to 72N/m, and 3111m/s to 3832m/s, respectively with the highest values exhibited by mix 100%GGBFS mix (Table 4). The incorporation of VA and VP reduced both UPV and fracture energy of AAMs as observed in the case of compressive strength.

Linear correlations exist between compressive strength ( $f_{cu}$ ) and density ( $\rho$ ) of the form:  $f_{cu} = 0.0535\rho - 71.388$  ( $R^2 = 0.5358$ ); between compressive strength and UPV of the form:  $f_{cu} = 0.0275UPV - 56.226$  ( $R^2 = 0.998$ ) and between fracture energy ( $G_f$ ) and compressive strength of the form:  $G_f = 0.753f_{cu} + 35.687$  ( $R^2 = 0.9874$ ) as presented in Figure 2. These linear relationships indicate that the

The SEM and EDS analyses were done on mortars to determine the reaction products. The specimens were taken from the core of the failed compression test cubes at 28 days for SEM/EDS analysis. The specimens were grounded and softly polished with sandpaper down to 30 $\mu$ m before a gold coating was done on the specimens to make the surface conductive.

## Results and Discussions

### Mechanical characteristics of mortars

The mechanical properties of the developed AAMs are evaluated in terms of dry density, compressive strength, UPV and fracture energy.

measurement of UPV (a non-destructive technique) can give some idea about the compressive strength of AAMs. This also proves the general hypothesis that the higher compressive strength resulted in higher fracture energy and UPV as well as higher density resulted in higher compressive strength (Figure 2).

The incorporation of VP also reduced the density of the mixes and 100%VP mix (VPM) satisfied the criteria for lightweight mix showing a density of 1825kg/m<sup>3</sup> (<1850kg/m<sup>3</sup>) (Table 4). The higher compressive strength associated with higher UPV and fracture energy of GGBFS incorporated AAMs compared to VA or VP incorporated ones can be attributed to the higher calcium content (as evident from the higher CaO/SiO<sub>2</sub> ranging in Table 3) related to the formation of C-A-S-H gels with traces of C-S-H. The main reaction products consisted of C-A-S-H and calcium-rich N-C-A-S-H binding phases as indicated in SEM/EDS graphs presented in Figure 3. Additional binding phase composed of C-S-H can also be observed in the SEM micrographs because of the higher calcium content in the system. The presence of the above-mentioned compounds can be confirmed from the presence of elements (Ca=17.6%, Si=13.4%, Al=4.5%, Na=5.9% and O=43.7%) noted in the EDS graph for SM (Figure 3a) and elements (Ca=8.2%, Si=12.7%, Al=4.1%, Na=5.6% and O=49%) in VAM (VA and VP based AAMs showed similar formation of binding phases) (Figure 3b). The partially hydrated GGBFS and VA/VP particles were also observed in the SEM micrographs.

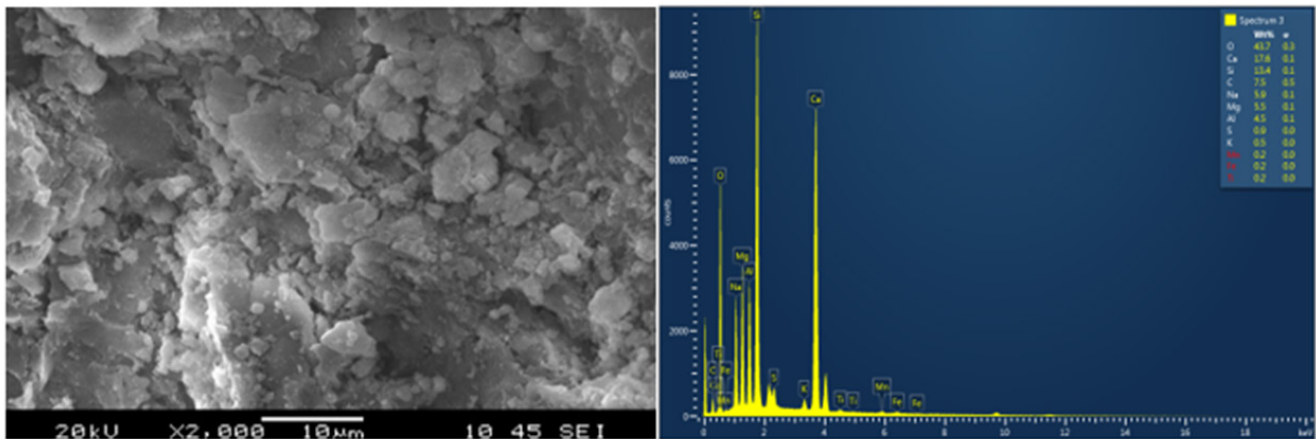


**Figure 3a:** SEM micrograph and EDS analysis of AAM with 100%GGBFS (SM).

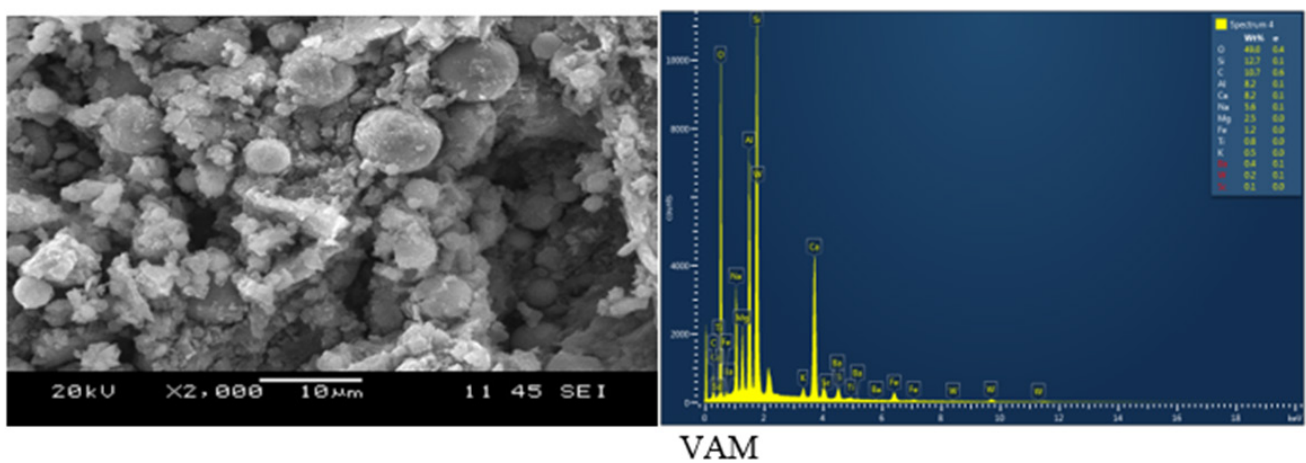


**Figure 3b:** SEM micrograph and EDS analysis of AAM with VA (VAM).

In general, AAMs with GGBFS exhibited a denser microstructure as evident from the SEM due to higher calcium content in the mix compositions resulting in better mechanical properties and durability properties in terms of compressive strength, fracture energy, water absorption and chloride permeability characteristics.

### Durability characteristics

The durability properties of AAMs are described based on drying shrinkage/expansion in water curing regime, sorptivity indices and the freeze-thaw resistance of specimens made of AAMs.

**Table 5:** Length and mass change of pastes and mortars in water curing regime.

AAM Mixes	Length change (%)		Mass change (%)		Initial sorptivity (mm/√s)	Secondary sorptivity (mm/√s)	Rapid chloride permeability, RCP	
	56d	90d	56d	90d			Coulombs	Class
SM	-0.55	-0.58	0.37	0.58	$1.7 \times 10^{-3}$	$3.6 \times 10^{-4}$	141	Very low
VAM	-0.38	-0.41	0.20	0.42	$2.4 \times 10^{-3}$	$4.5 \times 10^{-4}$	225	Very low
VPM	-0.35	0.42	0.19	0.40	$2.9 \times 10^{-3}$	$5.1 \times 10^{-4}$	425	Very low
VAVPM	-0.32	-0.40	0.18	0.35	$2.7 \times 10^{-3}$	$4.7 \times 10^{-4}$	400	Very low
VASM	-0.45	-0.47	0.26	0.46	$2.1 \times 10^{-3}$	$4.0 \times 10^{-4}$	180	Very low
VPSM	-0.43	-0.45	0.25	0.43	$2.3 \times 10^{-3}$	$4.2 \times 10^{-4}$	352	Very low

Negative (-) sign in length change indicates shrinkage and positive value of mass change denotes mass gain.

**Shrinkage/Expansion:** The length (shrinkage/expansion) and mass change of specimens made of AAMs were determined at 1,7,28,56, and 90 days. The length and mass change results at 56 and 90 days are presented in Table 5.

The variation in shrinkage/expansion strains for AAM specimens with time is presented in Figure 4. AAM mixes at all ages exhibited shrinkage (-ve values) at all ages. The 100%GGBFS mix (SM) showed higher shrinkage strain compared to those

incorporating VA or VP or their combination with GGBFS with VAVPM showing the lowest strain. The 90-day shrinkage strain ranged between 0.41% and 0.58% (Table 5). The incorporation of VA and VP as replacement of GGBFS exhibited the beneficial effect of reducing shrinkage strain. It seems to be that the rate of shrinkage strain reduced after 56 days. The presence of silica sand might have also reduced shrinkage strains because of the voids in the mortar mixes were filled by silica sand particles making the matrix denser

and more compact. Also, it can be attributed to the comparatively lower volume of pastes in the mortar mixes due to the addition of 30% silica sand. The combined effect of low reactive VA and VP particles and inert silica sand facilitated combating shrinkage strains by occupying the void spaces. The higher content of fly ash in alkali activated slag-fly ash-based mortars also exhibited lower shrinkage due to the dilution effect of fly ash inert filler in previous research studies [30].

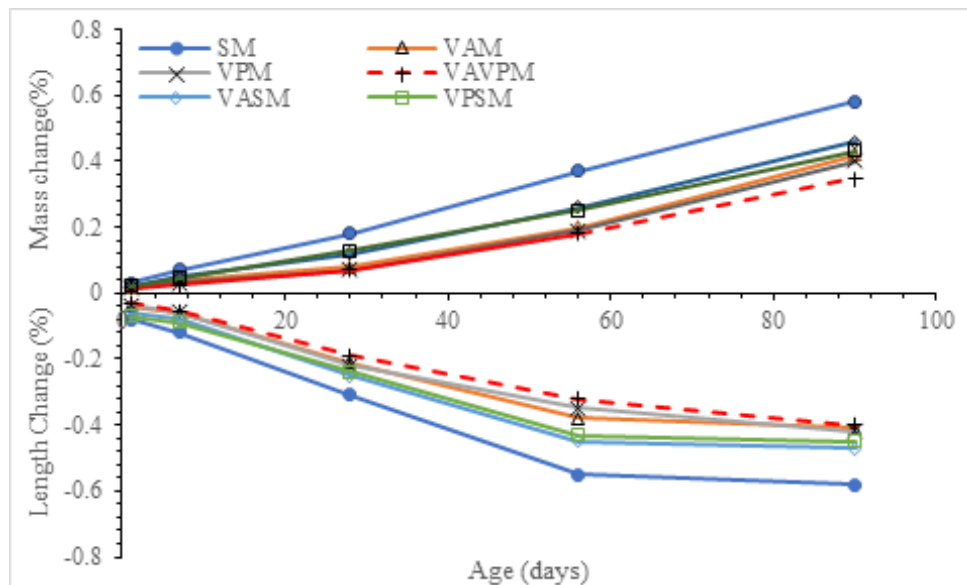


Figure 4: Variation of length and mass change of AAMs with age.

The variation in mass change for AAM specimens with time is presented in Figure 4. AAM mixes at all ages exhibited mass increase (+ve values) at all ages. The 100%GGBFS mix (SM) showed higher mass increase compared to those incorporating VA or VP or their combination with GGBFS with VAVPM showing the lowest mass increase. The AAMs with GGBFS exhibited higher mass increase (varying from 0.43% to 0.58% at 90 days with 100%GGBFS showing the highest value; Table 5) owing to the higher calcium content in the system than their VA or VP counterparts (ranging from 0.35% to 0.42% at 90 days, Table 5). This can be attributed to the higher calcium content in the GGBFS incorporated mixes resulted in the predominant formation of C-A-S-H and N-C-A-S-H gels with C-S-H.

**Water absorption/sorptivity and chloride ion permeability:** The water absorption characteristics defined by initial and secondary sorptivity indices of all the AAM mixes are presented in Table 5. The initial sorptivity indices ranged from  $1.7 \times 10^{-3} \text{mm}/\sqrt{s}$  to  $2.9 \times 10^{-3} \text{mm}/\sqrt{s}$  while secondary sorptivity ranged from  $3.6 \times 10^{-4} \text{mm}/\sqrt{s}$  to  $5.1 \times 10^{-4} \text{mm}/\sqrt{s}$  with 100%GGBFS mix (SM) showing the lowest and 100%VP mix (VPM) showing the highest values. The increase in VA and VP content increased both sorptivity indices. RCP values of AAMs based on the average of three-cylinder specimens are presented in Table 5. All the mixes are classified as very low based on ASTM C1202-22E01 (2022) ranging from 141 Coulombs to 425 Coulombs. Incorporation of VA or VP increased the RCP values of AAMs compared to their GGBFS

counterparts, but values remained within very low range. Similar range of results were found in previous studies [31]. VP-based AAMs exhibited higher sorptivity and RCP compared to their VA counterparts possibly due to lightweight and porous nature of VP. In general, AAMs with GGBFS exhibited a denser microstructure due to predominant formation of C-A-S-H and N-C-A-S-H gels with traces of C-S-H as evident from the SEM due to higher calcium content in the mix compositions resulting in lower sorptivity and RCP values.

## Conclusion

Ambient cured alkali-activated mortars (AAMs) were developed from combinations of precursors such as 100%VA, 100%VP, 50%VA+50%VP, 50%VA + 50%GGBFS, 50%VP+ 50%GGBFS and 100%GGBFS using a powder-based reagent combination (calcium hydroxide: sodium metasilicate=1:2.5) and a constant amount of silica sand. The main conclusions drawn from mechanical, durability, and microstructural analyses of the developed mortar compositions are as follows:

1. All AAMs satisfied the criteria for structural concrete with 28-day compressive strengths ranging from 29MPa to 49MPa with 100%VP incorporated mortar satisfied the criteria to be lightweight. Incorporation of VA and VP as replacement of GGBFS decreased the compressive strength, UPV and fracture energy of AAMs with VP incorporated mixes exhibiting lower

values compared to their VA counterparts. SEM/EDS analysis revealed the formation of C-A-S-H/N-C-A-S-H as the primary binding phases for mortars with traces of C-S-H. VA and VP incorporated mortars exhibited less dense microstructure compared to those with GGBFS due to lower calcium content and low reactivity of VA and VP.

- Linear correlations exist between compressive strength and density or UPV or fracture energy. Generally higher compressive strength resulted in higher fracture energy and UPV as well as higher density resulted in higher compressive strength.
- The VA and VP incorporated AAMs exhibited better shrinkage characteristics under water curing showing lower values compared to their GGBFS counterparts.
- The VA and VP incorporated mortars exhibited better higher initial and secondary sorptivity values as well as higher rapid chloride permeability compared to their GGBFS counterparts with VP mortar showing the higher values compared to their VA counterparts. This can be attributed to the lightweight and porous nature of VP. However, chloride permeability values of all AAMs are in the very low category and found satisfactory.
- This research demonstrated the viability of producing ambient cured powder based AAMs especially using volcanic materials (VA, VP or in combination of GGBFS) as green and sustainable alternatives to conventional cement-based mortars having satisfactory mechanical and durability characteristics. The developed AAMs can be used for structural applications.

## Acknowledgement

The authors gratefully acknowledge the financial support provided by Natural Science and Engineering Research Council (NSERC), Canada.

## References

- Garcia-Lodeiro I, Palomo A, Fernández-Jiménez A (2015) An overview of the chemistry of alkali-activated cement-based binders. Woodhead Publishing Limited, Cambridge, UK.
- Cengiz B, Giulia T, Hamada E, Enrico B (2023) Sustainable manufacturing of new construction material from alkali activation of volcanic tuff. *Materials Today Communications* 36: 106645.
- Provis JL (2018) Alkali-activated materials. *Cem Concr Res* 114: 40-48.
- Singh B, Ishwarya G, Gupta M, Bhattacharyya SK (2015) Geopolymer concrete: A review of some recent developments. *Constr Build Mater* 85: 78-90.
- Firdous R, Stephan D, Djobo JNY (2018) Natural pozzolan based geopolymers: A review on mechanical, microstructural and durability characteristics. *Constr Build Mater* 190: 1251-1263.
- Ding Y, Shi CJ, Li N (2018) Fracture properties of slag/fly ash-based geopolymer concrete cured in ambient temperature. *Constr Build Mater* 190: 787-795.
- Zhang S, Li Z, Ghiassi B, Yin S, Ye G (2020) Fracture properties and microstructure formation of hardened alkali-activated slag/fly ash paste. *Cem Concr Res* 144.
- Pan Z, Sanjayan JG, Rangan BV (2011) Fracture properties of geopolymer paste and concrete. *Magazine of Concrete Research*. 63(10): 763-771.
- Carolina A, Trindade C, Curoso I, Liebscher M, Mechtcherine V (2020) On the mechanical performance of K- and Na-based strain-hardening geopolymer composites (SHGC) reinforced with PVA fibers. *Constr Build Mater* 248: 01-16.
- Li Z, Liu J, Ye G (2019) Drying shrinkage of alkali-activated slag and fly ash concrete; A comparative study with ordinary Portland cement concrete. *Heron* 64(1/2): 01-15.
- Abdel-Gawwad HA, Abd El-Aleem S (2015) Effect of reactive magnesium oxide on properties of alkali activated slag geopolymer cement pastes. *Ceram Silikat* 59(1): 37-47.
- Adesanya E, Ohenoja K, Luukkonen T, Kinnunen P, Illikainen M (2018) One-part geopolymer cement from slag and pretreated paper sludge. *J Clean Prod* 185: 168-175.
- Castel A, Foster SJ, Ng T, Sanjayan JG, Gilbert RI (2016) Creep and drying shrinkage of a blended slag and low calcium fly ash geopolymer concrete. *Mater Struct Constr* 49(5): 1619-1628.
- Alnkaa A, Yaprak H, Memis S, Kaplan G (2018) Effect of different cure conditions on the shrinkage of geopolymer mortar effect of different cure conditions on the shrinkage of geopolymer mortar. *Int J Eng Res Dev* 14(10): 51-55.
- Thomas RJ, Lezama D, Peethamparan S (2017) On drying shrinkage in alkali-activated concrete: Improving dimensional stability by aging or heat-curing. *Cem Concr Res* 91: 13-23.
- Wardhono A, Gunasekara C, Law DW, Setunge S (2017) Comparison of long-term performance between alkali activated slag and fly ash geopolymer concretes. *Construction and Building Materials* 143: 272-279.
- Adesina A, Das S (2020) Drying shrinkage and permeability properties of fibre reinforced alkali-activated composites. *Constr Build Mater* 251: 01-09.
- Bernardo E, Elsayed H, Mazzi A, Tameni G, Gazzo SE (2022) Double-life sustainable construction materials from alkali activation of volcanic ash/discarded glass mixture. *Construction and Building Materials* 359: 129540.
- Moon J, Kim K, Yoon S, Bae S, Kim KS, et al. (2014) Characterization of natural pozzolan-based geopolymeric binders. *Cem Concr Compos* 53: 97-104.
- Játiva A, Ruales E, Etxeberria M (2021) Volcanic ash as a sustainable binder material: an extensive review. *Materials (Basel)* 14(5): 1302.
- Hossain KMA (2003) Blended cement using volcanic ash and pumice. *Cem Concr Res* 33: 1601-1605.
- Hossain KMA (2005) Volcanic ash and pumice as cement additives: Pozzolanic, alkali-silica reaction and autoclave expansion characteristics. *Cem Concr Res* 35: 1141-1144.
- Sood D, Hossain KMA (2021) Optimizing precursors and reagents for the development of alkali-activated binders in ambient curing conditions. *J Compos Sci* 5(2): 01-20.
- ASTM C109/C109 M (2016) Standard test method for compressive strength of hydraulic cement mortars (Using 2-in. or [50-mm] Cube Specimens), West Conshohocken, ASTM International, PA, USA.
- ASTM C157/C157M-17 (2017) Standard test method for length change of hardened hydraulic-cement mortar and concrete, West Conshohocken, ASTM International, PA, USA.
- ASTM C1585-13 (2013) Standard test method for measurement of rate of absorption of water by hydraulic-cement concretes, West Conshohocken, ASTM International, PA, USA.



27. ASTM C1202-22E01 (2022) Standard test method for electrical indication of concrete's ability to resist chloride ion penetration. West Conshohocken, ASTM International, PA, USA.
28. ACI Committee 318 (2019) Building code requirements for structural concrete and commentary, ACI 318-19, Farmington Hills, American Concrete Institute, MI, USA.
29. Karihaloo BL, Nallathambi P (1990) Effective crack model for the determination of fracture toughness ( $K_{Ic}^e$ ) of concrete. Eng Fract Mech 35(4-5): 637-645.
30. Punurai W, Kroehong W, Saptamongkol A, Chindapasirt P (2018) Mechanical properties, microstructure and drying shrinkage of hybrid fly ash-basalt fiber geopolymer paste. Constr Build Mater 186: 62-70.
31. Rajamane N, Nataraja M, Jeyalakshmi R (2014) Pozzolan industrial waste based geopolymer concretes with low carbon footprint. The Indian Concrete Journal 88(7): 49-68.